Available online at www.sciencedirect.com
SCIENCE DIRECT®
ELSEVIER
Physica D 183 (2003) 175–189
PHYSICA D
www.elsevier.com/locate/physd

Combustion initiation and extinction in a 2D chaotic flow

I.Z. Kiss [a,*], J.H. Merkin [a], Z. Neufeld [b]

[a] *Department of Applied Mathematics, University of Leeds, Leeds LS2 9JT, UK*
[b] *Center for Nonlinear Studies, Los Alamos National Laboratory, MS B268, Los Alamos, NM 87545, USA*

Received 11 December 2002; received in revised form 1 May 2003; accepted 8 May 2003
Communicated by L. Kramer

Abstract

The evolution of a flame in a reaction–advection–diffusion combustion system in the presence of chaotic stirring by an unsteady laminar fluid flow is considered. Two distinct regimes are found as the stirring rate is increased. When the reaction is slow (or fast stirring) localised temperature perturbations decay—the flame is quenched by the flow. If the reaction is fast (or slow stirring) a localised ignition leads to a stationary flame with complex filamental structure. The width of the filaments depends on the reaction and stirring rates. This problem is investigated numerically in 2D for an open flow system formed by two alternately opened point-vortex-sinks and the results are compared with previous results [Physica D 176 (1–2) (2003) 67–81] from a 1D 'mean-strain' model for the transverse profile of the flame filaments. The system is studied for different Lewis and Damköhler numbers, with a critical Damköhler number being found, dependent on the Lewis number, for the transition from trivial to combustion states. A comparison between time-periodic and steady flow regimes shows that chaotic motion of the fluid elements in the unsteady flow significantly enhances the combustion.
© 2003 Elsevier B.V. All rights reserved.

PACS: 82.33.Vx; 82.40.Ck; 05.45.−a

Keywords: Combustion; Chaotic mixing; Quenching; Stationary flame

1. Introduction

Understanding the behaviour of chemical and biological processes which take place within an imperfectly mixed (inhomogeneous) environment is an actively developing area of research at present, see [1–6] for example. Detailed studies include the mixing of reactants within continuously fed or batch reactors [1], the spread of plankton blooms within oceanic currents [3,5] and atmospheric dynamics [7]. Apart from their intrinsic theoretical interest these problems have a number of industrial applications such as chemical reactors, industrial burners, the study of engines and also in a range of geophysical problems. A 2D or 3D reaction–advection–diffusion system can be set up to describe this type of problem. However, huge computational power is necessary to perform any realistic numerical simulations. Any general information that can be obtained from simplified models of such systems is extremely

* Corresponding author. Fax: +44-113-343-5090.
E-mail address: istvan@maths.leeds.ac.uk (I.Z. Kiss).

0167-2789/$ – see front matter © 2003 Elsevier B.V. All rights reserved.
doi:10.1016/S0167-2789(03)00172-6

useful, as it can help explain the results obtained from numerical simulations as well as reducing the computational time considerably by highlighting those specific cases that should be considered.

One such method is that developed by Neufeld et al. [8,9] (see also [10–13] for earlier work) which suggests that a 1D model can be constructed if the advection in the system is chaotic [14,15]. Their idea is based on the fact that in a 2D chaotic flow we can assign to any point in the flow a convergent and a divergent direction associated with the eigenvectors corresponding to the negative and positive Lyapunov exponents of the chaotic advection. These directions are, respectively, tangent to the stable and unstable foliations of the advection dynamics [16]. Any advected material line tends to align along the unstable foliation in forward time, or along the unstable foliation in backward time. Thus, the stirring process smoothes out the concentration of the advected tracer along the stretching direction, whilst enhancing the concentration gradients in the convergent direction [17]. If we separate the original 2D reaction–advection–diffusion problem along the (Lagrangian) stretching and convergent direction we obtain a 1D equation for the average profile of the filament. This 1D model, called the 'Lagrangian filament model', retains the main features of the original system allowing us to obtain insight into the more general case.

Fluid mixing plays an important role in combustion [18–22]. In a previous paper [23], we studied in detail the 1D filament model for a simple combustion reaction. We found that there was a critical Damköhler number with Damköhler numbers greater than this being required to sustain combustion. This critical value is dependent on the Lewis number *Le*, increasing rapidly for small values of *Le* though being virtually constant at high *Le*. We also found that, for high Damköhler numbers, an inert, fully reacted core developed at the centre of the filament with the reaction then being at a distance away from the centre. The temperature within the filaments decreases as the Lewis number is increased and vice versa. These results from the 1D model guide our study of the 2D problem, in particular, in trying to identify critical Damköhler numbers and their dependence on the Lewis number.

Our aim is to consider the effect of chaotic mixing within a combustion reaction, which we model as a first-order process converting a fuel A to an inert product P through the reaction:

$$A \rightarrow P, \quad \text{rate} = ak(T) \tag{1}$$

with a positive exothermicity q. T is the (absolute) temperature and a is the concentration of reactant A. The temperature dependence of the reaction rate is given by an Arrhenius law with an ignition temperature T_i, namely

$$k(T) = \begin{cases} k_0 \exp\left(-\dfrac{E}{RT}\right) & \text{if } T > T_i, \\ 0 & \text{if } T \leq T_i, \end{cases} \tag{2}$$

where E and R are the activation energy and the universal gas constant and k_0 the (constant) pre-exponential factor. Our reason for choosing this form for the rate law is to avoid the difficulties associated with the cold boundary problem. An alternative approach is, rather artificially, to set the ambient temperature to zero. The form given by (2) allows for a non-zero ambient temperature and the discontinuity in $k(T)$ at $T = T_i$ does not lead to any particular problems in the numerical integrations provided T_i is kept small.

Considering the dynamics of the reaction schemes (1) and (2) it can be show that there are two steady states, $(T, a) = (T_\mathrm{a}, a_0)$ and $(T, a) = (T_\mathrm{b}, 0)$, where a_0 is the initial (uniform) concentration of A, T_a ($<T_i$) is the ambient temperature and $T_\mathrm{b} = T_\mathrm{a} + (qa_0/\rho C_p)$ is the burnt gas temperature. The two (spatially uniform) steady states correspond to the unreacted and fully reacted phases of the system.

Stirring is modelled by a simple time-periodic velocity field, representing an open flow system. The velocity field $\mathbf{v}(\mathbf{r}, t)$ is assumed to be independent of the concentration of the fuel and temperature. The results described in this paper are expected to be valid for a wide class of 2D time-dependent laminar flows, since the only requirement of our chosen flow field is that it produces chaotic motion of fluid elements. In our system, the reactant continuously

flows into and then out of a finite mixing zone with constant temperature T_a and reactant concentration a_0 being maintained at the inflow boundaries.

Advection in unsteady open flows has been shown to be governed by a chaotic scattering type escape process generating fractal patterns of the advected tracers [24–27]. The key ingredient to this is the existence of an invariant chaotic set formed by the union of all periodic and bounded aperiodic trajectories of fluid elements that bounce around the sinks but never escape. The stable manifold of this chaotic saddle (set of trajectories that come from infinity and end up on the saddle) is the boundary of the basins of attraction of the two point sinks. Such bounded 'non-escaping' trajectories are also typical of advection in unsteady flows formed in the wake of an obstacle [24,27]. Although the set of bounded orbits is unstable, typically a fractal set of measure zero, trajectories coming sufficiently close to the chaotic saddle can be trapped for arbitrarily long time around it before they escape along its unstable manifold. The unstable manifold of the chaotic saddle can be easily visualised by injecting a droplet of dye (ensemble of marked fluid particles) into the mixing zone. As the total amount of dye in the mixing zone decreases in time the remainder traces out the unstable manifold of the bounded chaotic set.

2. Governing equations

As an example of an open flow system we consider the velocity field around two alternately opened point-vortex-sinks in an unbounded 2D domain, the 'blinking vortex-sink' [26,28]. The fluid particles approach the mixing zone from infinity and leave the domain through either one of the sinks. The velocity field composed of the superposition of a point-vortex and a point-sink, is defined by the complex potential:

$$w(z) = -(C + \mathrm{i}K)\ \ln|z - z_s|, \tag{3}$$

where $z = x+\mathrm{i}y$, z_s ($z_s = (\pm\ell, 0)$) is the position of the active sink and C and K the sink-strength and vortex-strength, respectively. The velocity field corresponding to $w(z)$ consists of the superposition of a radial component $v_r = -C/r$ and of a tangential component $v_\phi = K/r$ with the origin fixed at the active sink, $r = \sqrt{(x - x_s)^2 + (y - y_s)^2}$. In Cartesian coordinates the velocity field can be written as

$$v_x = \frac{-Cx - Ky}{x^2 + y^2}, \qquad v_y = \frac{Kx - Cy}{x^2 + y^2}. \tag{4}$$

The equations for the 2D reaction–advection–diffusion problem are

$$\rho C_p \left(\frac{\partial T}{\partial t} + \mathbf{v} \cdot \nabla T \right) = \kappa \Delta T + qak(T), \tag{5}$$

$$\frac{\partial a}{\partial t} + \mathbf{v} \cdot \nabla a = D\Delta a - ak(T) \tag{6}$$

in $\mathbf{r} \in \Omega, t > 0$, where $\Omega = [-L/2, L/2] \times [-L/2, L/2]$ is a square of size L covering the mixing zone. Here ρ is the density, C_p the specific heat and κ, D are, respectively, the thermal conductivity and diffusion coefficient. Eqs. (6) and (7) are subject to the boundary conditions that

$$T(\mathbf{r}, t) = T_a, \qquad a(\mathbf{r}, t) = a_0 \quad \text{on} \quad \mathbf{r} \in \partial\Omega \quad (t > 0). \tag{7}$$

We are interested in the response of the system, initially in the homogeneous trivial steady state $T = T_a$ and $a = a_0$, to a localised perturbation in a form of a heat input ($T > T_i$) added to the system at $t = 0$. By localised we mean that the spatial extent of the perturbation is much smaller then the characteristic size of the mixing zone.

In order to make Eqs. (5) and (6) non-dimensional, we introduce the following transformation:

$$\bar{T} = \frac{T - T_a}{T_b - T_a}, \qquad \bar{a} = \frac{a}{a_0}, \qquad \bar{t} = \frac{t}{T_0}, \qquad \bar{\mathbf{r}} = \frac{\mathbf{r}}{\ell}, \tag{8}$$

where T_0 and ℓ are the period of the flow and the half-distance separating the two sinks. This leads to the dimensionless equations, on dropping the bars for convenience:

$$\frac{\partial T}{\partial t} + \left(\frac{-\eta x - \eta\xi y}{x^2 + y^2}\right)\frac{\partial T}{\partial x} + \left(\frac{\eta\xi x - \eta y}{x^2 + y^2}\right)\frac{\partial T}{\partial y} = DaK(T)a + Pe^{-1}Le\Delta T, \tag{9}$$

$$\frac{\partial a}{\partial t} + \left(\frac{-\eta x - \eta\xi y}{x^2 + y^2}\right)\frac{\partial a}{\partial x} + \left(\frac{\eta\xi x - \eta y}{x^2 + y^2}\right)\frac{\partial a}{\partial y} = -DaK(T)a + Pe^{-1}\Delta a, \tag{10}$$

where

$$Da = k_0 T_0, \qquad Pe = \frac{\ell^2}{DT_0}, \qquad Le = \frac{\kappa}{D\rho c_p}, \qquad \eta = \frac{CT_0}{\ell^2}, \qquad \xi = \frac{K}{C} \tag{11}$$

are the Damköhler, Péclet and Lewis numbers, respectively. η and ξ are the dimensionless sink strength and the ratio of the vortex to sink strength. The parameters η and ξ were kept at the same values of $\eta = 1.0$ and $\xi = 10.0$ for all our numerical simulations, as suggested by Károlyi and Tél [26]. The temperature dependence of the reaction (2) becomes

$$K(T) = \begin{cases} \exp\left(-\dfrac{1}{\epsilon((1-\beta)T + \beta)}\right) & \text{if } T > \bar{T}_i, \\ 0 & \text{if } T \le \bar{T}_i, \end{cases} \tag{12}$$

where

$$\epsilon = \frac{RT_b}{E}, \qquad \beta = \frac{T_a}{T_b}, \qquad \bar{T}_i = \frac{T_i - T_a}{T_b - T_a}.$$

The boundary conditions to be applied are

$$T(\mathbf{r}, t) = 0, \qquad a(\mathbf{r}, t) = 1 \quad \text{on} \quad \mathbf{r} \in \partial\Omega \quad (t > 0). \tag{13}$$

The Damköhler number, *Da*, characterises the ratio between the advective and the chemical time-scales, large *Da* corresponds to slow stirring or equivalently fast chemical reaction and vice versa. The Péclet number, *Pe*, is a measure of the relative strength of advective and diffusive transport. We consider only large Péclet numbers, typical of many applications where advective transport dominates.

3. Numerical results

The reaction–advection–diffusion problem (9), (10) and (13) was integrated on a 1000×1000 square lattice using operator splitting method combining ADI (alternate–direction–implicit method) for advection and diffusion with a fourth-order Runge–Kutta for the time integration of the local chemical dynamics. The non-dimensionalisation (8) fixes the time period and the half-distance between the sinks, both as unity. Consistent with having a strongly advective flow we took a large value for the Péclet number, keeping it constant at $Pe = 2000$ and, following [23], we took $\epsilon = 1.0$, $\beta = 0.1$ and $\bar{T}_i = 0.001$. We fix the value of the Lewis number in the range 0.5 up to 10.0 and then vary the value of the Damköhler number for this particular value of *Le*. All our results are for square of side $L = 6.0$ ($\Delta x = \Delta y = 0.006$) and we used a time step $\Delta t = 0.0005$. We note that, varying the Damköhler number

while keeping the Péclet number fixed, corresponds to varying the chemical reaction rate. This procedure cannot be achieved by just changing the stirring rate (except in the rather artificial case of changing the diffusivity as well to keep *Pe* constant).

We find that there are two distinct regimes separated by a critical Damköhler number, Da_{crit}. In the slow reaction/fast stirring regime ($Da < Da_{\text{crit}}$) the flame is quenched by the flow and the initial perturbation decays towards a homogeneous steady state with $T = 0$ and $a = 1$ everywhere. When $Da > Da_{\text{crit}}$, the localised perturbation can persist and propagate in the form of a thin filament. However, this filament cannot fill the whole domain uniformly because of the continuous outflow of burnt gas and the inflow of fresh reactant. After an initial transient period a spatially non-uniform periodic state sets in, with the mixing zone partly covered by a complex filamental structure (steady flame). In our case, the final patterns vary periodically with the period of the flow and effectively take the same form about each open sink (see Fig. 3).

We start by determining the critical Damköhler number for a given value of *Le*. If the numerical simulations are performed with a fixed initial temperature input, when *Da* is close to Da_{crit}, it becomes difficult to generate a steady flame, since the attraction domain of the non-trivial steady state (steady flame) gets smaller as Da_{crit} is approached from above. Thus this approach leads to overestimates in the value of Da_{crit}. To avoid this problem, we started by first finding a Damköhler number which gave a non-trivial steady state from a simple initial perturbation. When the steady state had been reached (to well within numerical accuracy), we saved this data and used it as the initial condition for the next run in which the Damköhler number is slightly decreased. If, in the new run, we did not get extinction then this procedure is repeated until we did get extinction. The critical Damköhler number could then be fixed between the values of *Da* used for the final two runs.

We illustrate this in Fig. 1, where the average temperature $\langle T \rangle$ is plotted against t, for runs with *Da* around the critical value for $Le = 0.5$ and 10.0. Here

$$\langle T \rangle(t) = \frac{1}{L^2} \iint_{\Omega} T(x, y, t)\, \mathrm{d}x\, \mathrm{d}y. \tag{14}$$

In each case for supercritical Damköhler numbers, the mean temperature reaches a stationary state having small amplitude oscillations around a mean that depends on *Da*. The oscillations result from the oscillatory nature of the flow and have period $T/2$, that is half of the period of the flow (this is due to the symmetry property $T(x, y, t) = T(-x, -y, t + T/2)$ of the temperature field in the stationary state). When the Damköhler number is below the critical value the mean temperature decays to zero indicating the extinction of the flame. In Fig. 2a, we present the largest values of *Da* for extinction (lower curve) and the lowest values of *Da* for a stationary flame (upper curve) for a range of values of the Lewis number *Le*. The critical Damköhler number Da_{crit} lies between the two curves plotted in Fig. 2a. The increase in Da_{crit} with *Le* is consistent with our 1D filament model calculations [23], which show a strong increase in Da_{crit} for relatively small values of *Le* but a much slower increase in Da_{crit} for higher values of *Le*.

Starting our computations by using a previously established steady flame solution as initial conditions gives a critical Damköhler number independent of the form and position of the initial perturbation. Thus a steady flame will form for any $Da > Da_{\text{crit}}$ provided the initial perturbation is sufficiently large and the system will fail to ignite if $Da < Da_{\text{crit}}$. However, a steady flame may fail to ignite even for $Da > Da_{\text{crit}}$ if the initial perturbation is too small. To illustrate this point, we took an initial temperature input with a fixed amplitude but variable width δ of the form $T(\mathbf{r}, t = 0) = \exp(-((x - x_0)^2 + (y - y_0)^2)/2\delta^2)$ and obtained estimates of the minimum Damköhler number needed to sustain the flame, $Da_{\min}(\delta)$ ($Da_{\text{crit}} \equiv \min(Da_{\min}(\delta))$), for different values of δ ($Le = 1.0$ and all parameters are the same as the ones used in the other numerical simulations). With a given δ, by slowly decreasing the value of *Da* in successive runs, we obtained the smallest value for *Da* which resulted in a steady flame and the largest value which led to extinction, represented by full and dotted lines, respectively, in Fig. 2b. This measurement

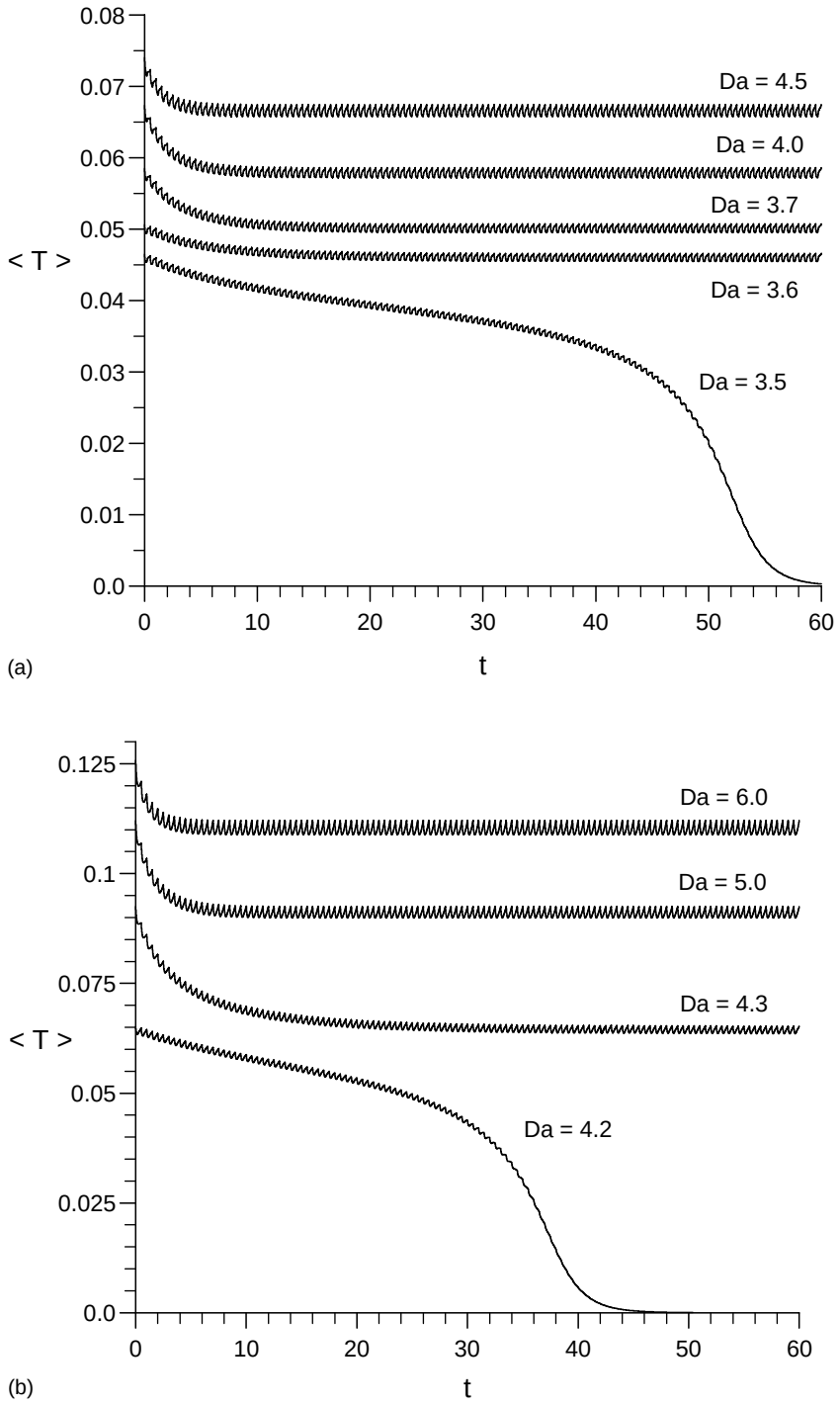

Fig. 1. Average temperature $\langle T \rangle$ (defined by (14)) plotted against t for: (a) $Le = 0.5$, (b) $Le = 10.0$, for values of Da noted on the figures. In each case $Pe = 2000$, $\epsilon = 1.0$, $\beta = 0.1$, $\bar{T}_i = 0.001$, $L = 6$.

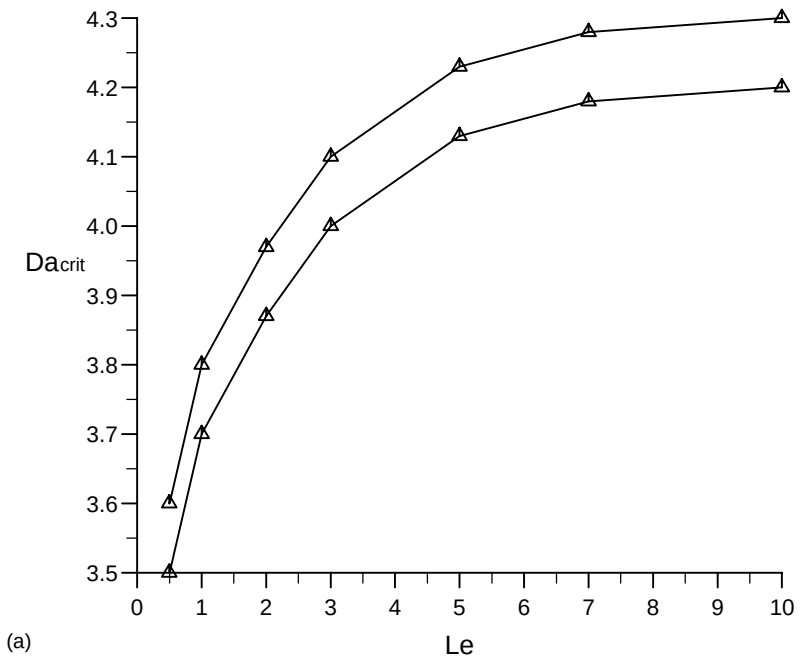

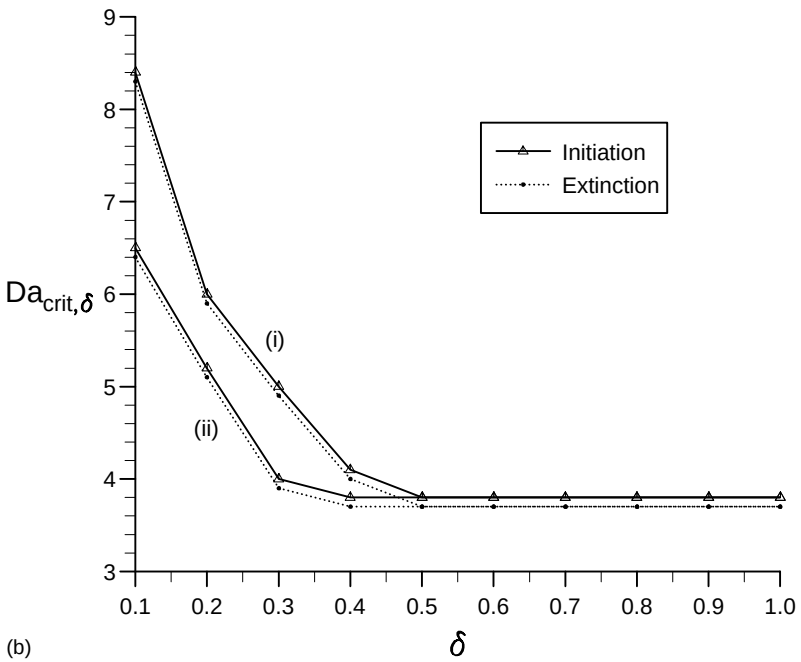

Fig. 2. (a) Dependence of the critical Damköhler number, Da_{crit}, on the Lewis number Le. The lower and upper curve represents the largest and the smallest values of Damköhler number Da for extinction and for a stationary flame, respectively. (b) Upper and lower bounds for the critical Damköhler number, $Da_{\text{crit},\delta}$, calculated for the initial perturbation $\exp(-((x-x_0)^2+(y-y_0)^2)/2\delta^2)$ centred in ($x_0=0$, $y_0=0$) graph (i) and ($x_0=0$, $y_0=1$) graph (ii) for $Le=1.0$ plotted against δ.

Table 1
Critical Damköhler numbers, Da_{crit}, estimated from the 2D model and obtained for the 1D Lagrangian filament slice model [23] for different Lewis numbers, Le

Le	Da_{crit}		Ratio
	2D	1D	
0.5	3.5–3.6	6.139	0.578
1.0	3.7–3.8	6.963	0.538
2.0	3.87–3.97	7.711	0.508
3.0	4.0–4.1	8.038	0.503
5.0	4.13–4.23	8.302	0.503
7.0	4.18–4.28	8.401	0.503
10.0	4.2–4.3	8.461	0.502

was repeated for two identical initial heat inputs centred in two different points of the domain, ($x_0 = 0.0$, $y_0 = 0.0$) and ($x_0 = 0.0$, $y_0 = 1.0$). For sufficiently large radius of the heat input, $\delta \geq 0.5$ and $\delta \geq 0.4$, respectively, $Da_{min}(\delta)$ is independent of δ and is the same as Da_{crit} (see Fig. 2a and Table 1). However, for smaller values of δ a higher value of Da is needed to initiate a steady flame. This value increases considerably for small δ.

We can compare the values of Da_{crit} estimated for the present model with those obtained from the 1D filament model [23]. The results are shown in Table 1, together with the ratio of the two values of Da_{crit} for a particular value of Le. (For the 2D model we took the mid value of the two values obtained from the numerics, the smallest Da for a stationary flame and the largest Da for extinction.) This ratio gives an estimate of an effective strain rate resulting from the advection ($\lambda_{eff} \approx 0.5$) in the 2D flow, which should be independent of Le. Though there are some variations in the ratios for the different Lewis numbers used in the numerical simulations, these are not too large and suggest that the Lagrangian filament model can provide a reliable guide for the 2D model. We note, that our value for the effective strain rate ($\lambda_{eff} \approx 0.5$) appears to be much smaller than the Lyapunov exponent of the advection ($\lambda = 2.19$) obtained for the same flow parameters in [26]. The main reason for this is likely to be the strong temporal fluctuations of the strain experienced along the path of a fluid element, whose effect is not equivalent to a constant averaged strain. Also a basic assumption behind the filament model is that the filaments are long and have little curvature, that is only a reasonable approximation for the 2D model (see Fig. 3).

In Fig. 3, we give a sequence of grey-level temperature plots for $Le = 0.5$ and $Le = 10.0$, in each case $Da = 8.0$ (well above the corresponding Da_{crit}). In these figures, the lighter colours correspond to higher temperatures. The basic development of the temperature field is qualitatively the same in each case. Each sequence starts at $t = 0$ with the initial perturbation in the temperature applied between the two sinks. The first set of plots are at equal time intervals corresponding to the opening of one sink and the closing of the other. This sequence shows a spiral filament structure developing around the open sink (2nd plot) resulting from the vortex motion around the open sink. As this sink closes these higher temperatures are pulled towards the other, now open, sink (3rd plot) initiating a reaction towards this sink. The spiral temperature filaments that formed around the second sink are then pulled towards the first as this one opens (4th plot) with relatively high temperatures developing in the region around this sink. This process continues with spiral temperature filaments forming around the open sink and regions of relatively high temperatures left near the closed sink until a periodic response is set up, see the 7th, 8th and 9th plots at $t = 4.0$, 5.5 and 8.0 corresponding to alternative openings of the sinks (second sink at $t = 4.0$, 8.0, first at $t = 5.5$).

The final time-periodic temperature field is essentially the same about each sink, the effect of opening one sink and closing the other is to move the spiral filaments to the region around the open sink and leave a larger region of high temperatures at the now closed sink, with the final structure reflected about the line joining the sinks. Thus the effect of the periodic flow is to move the reaction (and regions of high temperature) around the domain with

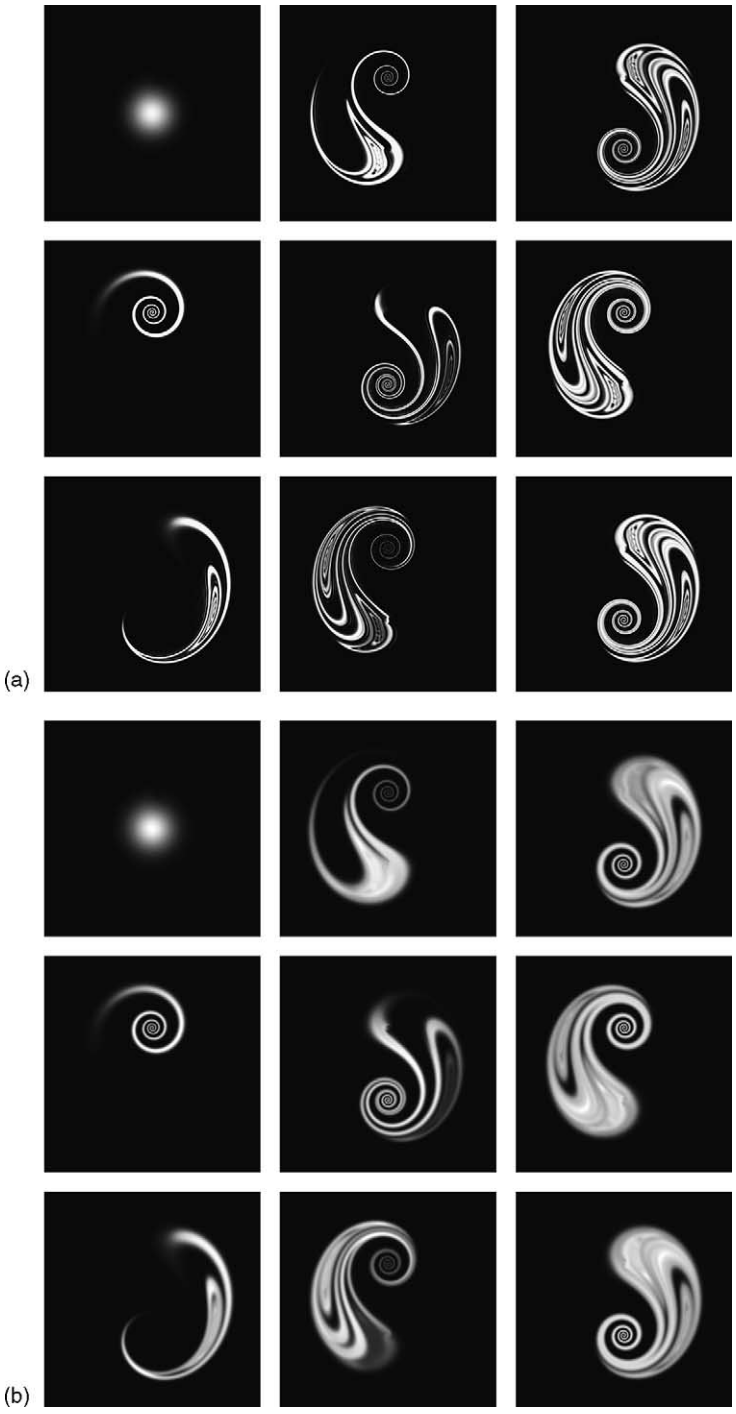

Fig. 3. Grey-level temperature plots (the lighter colours correspond to higher temperatures) for $Da = 8.0$ and (a) $Le = 0.5$, (b) $Le = 10.0$. In each case $Pe = 2000$, $\epsilon = 1.0$, $\beta = 0.1$, $\bar{T}_i = 0.001$, $L = 6$.

different regions reacting at different parts of the opening/closing sequence. The temperatures developed locally are sufficiently high to initiate reactions in the inert regions as they are moved around by the flow.

Differences are seen for low (Fig. 3a) and high (Fig. 3b) Lewis number. In the former cases, the filaments are relatively thin and are more clearly defined than in the latter case, in which they appear more 'diffuse'. This could be expected as high *Le* corresponds to high thermal diffusivity and the picture is consistent with the profiles seen in the 1D model [23]. In [23] the width of the temperature profiles increased in extent as *Le* was increased, for a given value of *Da*. This can also be seen in Fig. 4, where we plot the average temperature $\langle T \rangle$ against *Da* for $Le = 0.5$ and $Le = 10.0$. $\langle T \rangle$ was calculated from the final time-periodic solutions. The figure shows a much more rapid increase in $\langle T \rangle$ for the higher value of *Le*, again consistent with [23], and corresponds to having a thicker filament structure for larger *Le*. Our 2D numerical simulations can calculate only the stable solutions. However, the curves plotted in Fig. 4 show strong evidence for the saddle-node bifurcations at Da_{crit} seen in [23].

To characterise the structure of the flame filaments we also calculated the probability density functions (pdf) of the temperature for the final time-periodic flames. The pdf were computed by first determining the maximum and minimum temperatures in the steady flame. The range between these two values was divided into *n* equal parts (bins) and then, by going through the discretised temperature distribution, the number of temperature values which fall into a particular bin were counted. These numbers were normalised by dividing by the total number of grid points in the discretisation. The pdf are presented in Fig. 5 for $Da = 8.0$ and $Le = 0.5, 1.0, 10.0$. The largest temperatures, corresponding to the central parts of the filaments, are smaller than the burnt gas temperature, $T_{\mathrm{b}} \equiv 1.0$, for the larger Lewis number, and the maximum temperatures are higher than the burnt gas temperature when $Le < 1$, as predicted by the filament model [23]. The pronounced peak in the pdf at $T \approx 0.85$ for $Le = 10.0$ indicates the presence of a constant temperature plateau in the centre of the filaments. This has also been found to be a characteristic feature of the temperature profiles obtained from the filament model for larger Lewis numbers.

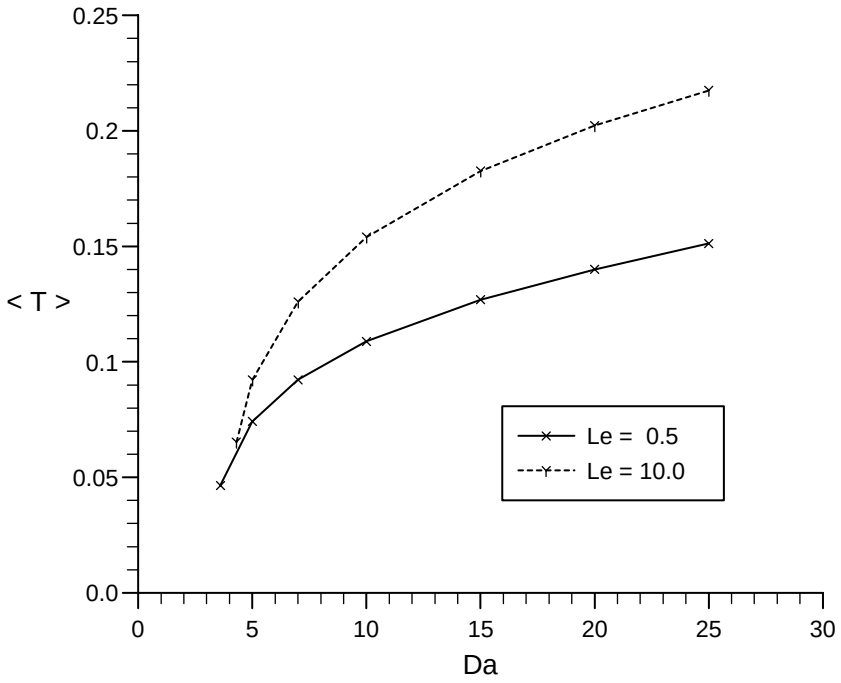

Fig. 4. Average temperature $\langle T \rangle$ (as defined in (14)) of the stationary flame structure as a function of Damköhler number *Da* for $Le = 0.5$ and $Le = 10.0$.

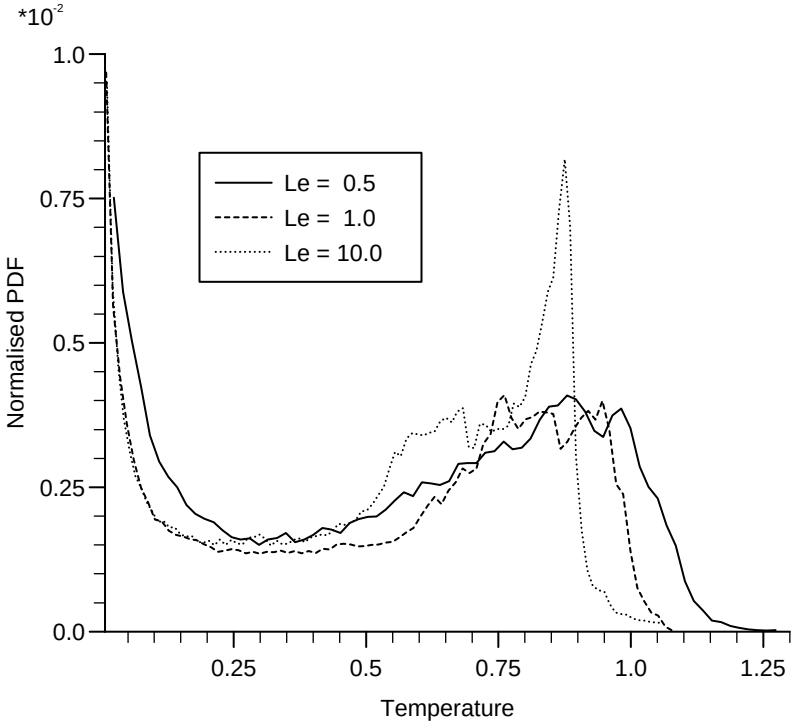

Fig. 5. Probability density functions (pdf) of the temperature in the stationary flame for $Da = 8.0$ and $Le = 0.5, 1.0, 10.0$.

We also note that, although larger temperatures are reached for small Lewis numbers, the average temperature $\langle T \rangle$ increases with Lewis number. This can be seen in Fig. 6, where we plot $\langle T \rangle$ against Le for $Da = 8.0$ and $Da = 16.0$. This increase in $\langle T \rangle$ with Le results from the growth in the spatial extent of the flame filaments, which appears to be more significant than the change in the maximum temperature reached at the centre of the filaments.

Finally, to investigate the role of chaotic advection in the combustion process we removed the time dependence of the velocity field by keeping both vortex-sinks open at all times. In this time-independent flow field, the fluid elements move along the streamlines and there are no chaotic fluid trajectories. The velocity field has a single hyperbolic fixed point ($x = 0$, $y = 0$) which is the only point that never leaves the system. This is the analogue of the chaotic saddle of the time-dependent flow. Keeping all parameters unchanged and $Le = 1.0$ we carry out the same numerical experiments as in the chaotic flow case. We find that there is again a critical Damköhler number, below which the flame is quenched. The critical value is found to be much higher than in the time-periodic flow, $Da_{\text{crit}} \approx 135$. This is because the rather large eigenvalues of the hyperbolic fixed point $(-20.1, 20.1)$ correspond to a very strong stretching capable of quenching the initial heat input. For supercritical Damköhler numbers, a steady flame forms along the unstable manifold of the fixed point $(0, 0)$ (Fig. 7). The dependence of the mean temperature of the stationary flame structure, $\langle T \rangle$ on Da is plotted in Fig. 8 and is qualitatively similar to the chaotic case (see Fig. 4). A striking difference, however, is that the values of $\langle T \rangle$ are very much lower. This is a consequence of the much smaller area of the flame in the absence of the chaotic saddle. This comparison shows that the existence of infinitely many bounded orbits in the presence of chaotic advection by a time-dependent flow makes the combustion process significantly more efficient. Note that both bounded sets, the chaotic saddle and the single hyperbolic fixed point of the time-independent flow, occupy a zero area. This suggests that an indicator of the mixing efficiency relevant for the combustion process could be the fractal dimension of the chaotic saddle, which is always zero for non-chaotic flows.

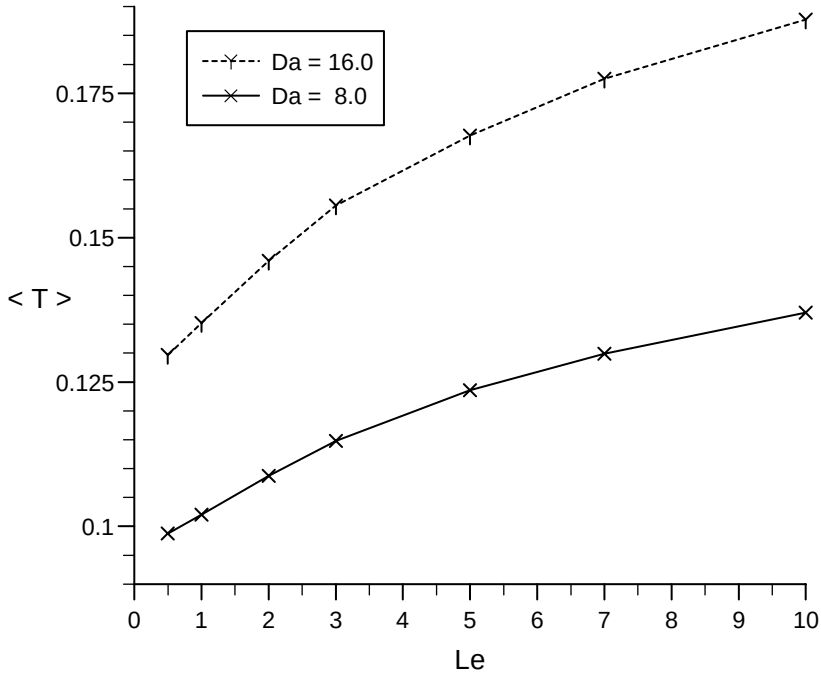

Fig. 6. Average temperature $\langle T \rangle$ (as defined in (14)) plotted against Le for $Da = 8.0$ and $Da = 16.0$.

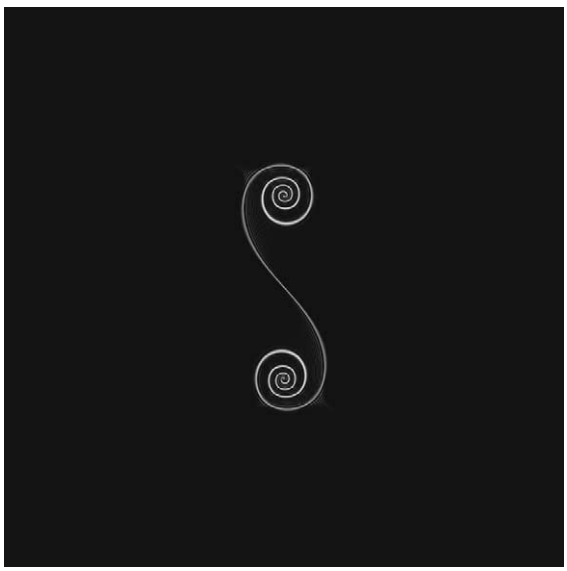

Fig. 7. Grey-level temperature plots (the lighter colours correspond to higher temperatures) in the steady flow regime for $Da = 150.0$, $Le = 1.0$, $Pe = 2000$, $\epsilon = 1.0$, $\beta = 0.1$, $\bar{T}_i = 0.001$, $L = 6$.

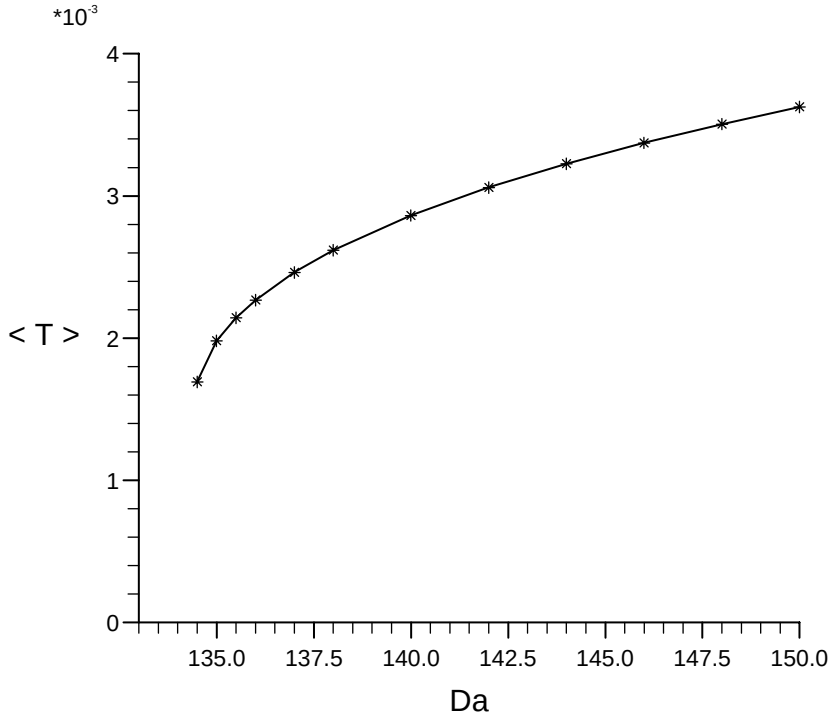

Fig. 8. Average temperature $\langle T \rangle$ (as defined in (14)) of the stationary flame structure in the steady flow regime as a function of Damköhler number *Da* for $Le = 1.0$.

4. Conclusions

The 2D model shows that a periodic filament structure (steady flame) can form in an open chaotic flow due to the interaction between the propagation of a reaction–diffusion front and the stretching due to chaotic advection. We have identified critical Damköhler numbers for different values of the Lewis number. Values of *Da* higher than these being necessary for fully developed flame propagation. The formation of a flame also depended on the initiation process. Even at values of *Da* larger than the critical values flames could still be extinguished by the flow if the initial perturbation in the temperature was insufficient. This effect became more noticeable close to criticality. The flames that do form have a thin filament structure (dependent on the Lewis number) with regions of high temperature interspersed with regions of lower temperatures (see Fig. 3). The effect of the periodic flow is to move the regions where the system is reactive and where it is effectively inert around the reactor, turning the reaction on or off at a particular point as the flow field changes.

The temperature distribution can be interpreted as a direct product of the temperature profile resulting from the filament model [23] (which represents the flow as a steady strain flow) and the unstable manifold of the chaotic saddle formed by the set of bounded trajectories of fluid elements [24,26]. These types of structure have been observed previously for autocatalytic reactions in open chaotic flows [8,29]. In our case, the chaotic saddle is the support of the flame, in the sense that the bounded trajectories keep the flame in the mixing zone.

It is interesting to note that the *attractor* of the advection–reaction–diffusion problem—the stationary flame structure—is centred around an unstable object, the *repellor* of the advection problem and its unstable manifold. The explanation of this apparent contradiction lies in the difference between the Lagrangian representation describing

the motion of fluid elements, and the Eulerian representation used to describe the evolution of the concentration fields. The stationary (time-periodic) attractor of the temperature distribution, is formed by continuously changing fluid elements as fresh fuel enters the reaction zone along the stable manifold of the chaotic saddle and burned gases within the filaments leave the system along the unstable manifold.

The width of the flame filaments decreases for small Damköhler numbers. In case of very thin filaments ($Da < Da_{\mathrm{crit}}$), the heat loss becomes important and therefore a stationary flame cannot be sustained. The thermal diffusivity is proportional with the Lewis number and this explains the increase of the critical Damköhler number with Lewis number.

Our study of the 2D problem was motivated by our previous work on the 1D Lagrangian filament model [23]. This latter model is very much easier to implement and showed the existence of critical Damköhler numbers and how these varied with *Le*, for example. It also gave information as to how the filament structures in temperature and concentration varied as the values of *Da* and *Le* were changed. What we see in the 2D problem agrees qualitatively, at least, with what was found in the 1D model. The basic assumption behind this 1D model that the filaments were thin and essentially straight is not fully realised in the 2D simulations, though it is a better approximation at the lower *Le* values (see Fig. 3a and b). The quantitative agreement between the two models that we tried to obtain was not especially strong (Table 1), but it does give some expectation that the Lagrangian filament approach should be a useful indicator as to how general reactive chaotic advection problem behave.

Finally, we note that an advantage of using the 1D filament model is that it gives access to a much greater range of values for the parameters *Da* and *Le*. In most applications the value of Péclet number is relatively large. In numerical simulations however, large values of Péclet number *Pe* forces small time Δt and space steps Δx, Δy (we took $\Delta x = \Delta y$). This becomes more pronounced at the more extreme values for *Da* or *Le*. For small values of *Le*, for example, the thinness of the filament structure needs very small space steps for its accurate resolution, this limits the value of *Le* to $Le \geq 0.5$ for which we could get reliable numerical results within reasonable computational times.

Acknowledgements

We wish to acknowledge the support of the ESF Programme REACTOR and I.Z. Kiss wishes to thank ORS and the University of Leeds for financial support.

References

[1] I.R. Epstein, The consequences of imperfect mixing in autocatalytic chemical and biological systems, Nature 374 (1995) 321–327.
[2] Z. Toroczkai, T. Tél (Eds.), Focus issue: Active Chaotic Flow, Chaos 12 (2) (2002) 372–530.
[3] E.R. Abraham, The generation of plankton patchiness by turbulent stirring, Nature 407 (2000) 695–702.
[4] G. Károlyi, Á. Péntek, I. Scheuring, T. Tél, Z. Toroczkai, Chaotic flow: the physics of species coexistence, Proc. Natl. Acad. Sci. USA 97 (2000) 13661.
[5] Z. Neufeld, P.H. Haynes, V. Garcon, J. Sudre, Ocean fertilization experiments may initiate large scale phytoplankton bloom, Geophys. Res. Lett. 29 (2002).
[6] W.R. Young, A.G. Roberts, G. Stuhne, Reproductive pair correlations and the clustering of organisms, Nature 412 (2001) 328–331.
[7] S. Edouard, B. Legras, F. Lefévre, R. Eymard, The effect of small-scale inhomogeneities on ozone depletion in the Arctic, Nature 384 (1996) 444–447.
[8] Z. Neufeld, P.H. Haynes, T. Tél, Chaotic mixing induced transitions in reaction–diffusion systems, Chaos 12 (2002) 426–438.
[9] Z. Neufeld, Excitable media in a chaotic flow, Phys. Rev. Lett. 87 (2001) 108301–108304.
[10] W.E. Ranz, Application of a stretch model to mixing, diffusion and reaction in laminar and turbulent flows, AIChE J. 25 (1979) 41–47.
[11] F.J. Muzzio, J.M. Ottino, Evolution of a lamellar system with diffusion and reaction: a scaling approach, Phys. Rev. Lett. 63 (1989) 47–50.
[12] I.M. Sokolov, A. Blumen, Mixing effects in the $A + B$ reaction–diffusion scheme, Phys. Rev. Lett. 66 (1991) 1942–1945.

[13] M.J. Clifford, S.M. Cox, E.P.L. Roberts, Lamellar modelling of reaction, diffusion and mixing in a two-dimensional flow, Chem. Eng. J. 71 (1998) 49–56.
[14] H. Aref, Stirring by chaotic advection, J. Fluid Mech. 143 (1984) 1–21.
[15] J.M. Ottino, The Kinematics of Mixing: Stretching, Chaos and Transport, Cambridge University Press, Cambridge, 1989.
[16] M. Giona, A. Adrover, F.J. Muzzio, S. Cerbelli, M. Alvarez, The geometry of mixing in time-periodic chaotic flows. I. Asymptotic directionality in physically realizable flows and global invariant properties, Physica D 132 (1999) 298–324.
[17] F. Városi, T.M. Antonsen, E. Ott, The spectrum of fractal dimensions of passively convected scalar gradients in chaotic fluid flows, Phys. Fluids A 3 (1991) 1017–1028.
[18] N. Peters, Turbulent Combustion, Cambridge University Press, Cambridge, 2000.
[19] P. Constantin, A. Kiselev, A. Oberman, L. Ryzhik, Bulk burning rate in passive-reactive diffusion, Arch. Ration. Mech. 154 (2000) 53–91.
[20] M. Abel, A. Celani, D. Vergni, A. Vulpiani, Front propagation in laminar flows, Phys. Rev. E 64 (2001) 46307.
[21] A. Kiselev, L. Ryzhik, Enhancement of the travelling front speeds in reaction–diffusion equations with advection, Ann. I.H. Poincaré 18 (2001) 309–358.
[22] P. Constantin, A. Kiselev, L. Ryzhik, Quenching of flames by fluid advection, Commun. Pure Appl. Math. 54 (2001) 1320–1342.
[23] I.Z. Kiss, J.H. Merkin, S.K. Scott, P.L. Simon, S. Kalliadasis, Z. Neufeld, The structure of flame filaments in chaotic flows, Physica D 176 (1–2) (2003) 67–81.
[24] E. Ziemniak, C. Jung, T. Tél, Physica D 76 (1994) 76.
[25] Á. Péntek, T. Tél, Z. Toroczkai, J. Phys. A 28 (1995) 2191.
[26] G. Károlyi, T. Tél, Chaotic tracer scattering and fractal basin boundaries in a blinking vortex-sink system, Phys. Rep. 290 (1997) 125–147.
[27] J.C. Sommerer, H.C. Ku, H.E. Gilreath, Experimental evidence for chaotic scattering in a fluid wake, Phys. Rev. Lett. 77 (1996) 5055–5058.
[28] H. Aref, S.W. Jones, S. Mofina, I. Zawadski, Physica D 37 (1989) 423.
[29] Z. Toroczkai, Gy. Károlyi, Á. Péntek, T. Tél, C. Grebogi, Advection of active particles in open chaotic flows, Phys. Rev. Lett. 80 (1998) 500–503.